11th World Congress on Computational Mechanics (WCCM XI)
5th European Conference on Computational Mechanics (ECCM V)
6th European Conference on Computational Fluid Dynamics (ECFD VI)
E. Oñate, J. Oliver and A. Huerta (Eds)

COMBINATION OF INTERSECTION- AND SWEPT-BASED METHODS FOR SINGLE-MATERIAL REMAP

MATĚJ KLÍMA*, MILAN KUCHAŘÍK* AND MIKHAIL SHASHKOV†

*Faculty of Nuclear Sciences and Physical Engineering (FNSPE)
Czech Technical University in Prague
Břehová 7, Praha 1, 115 19, Czech Republic
e-mail: klimamat@fjfi.cvut.cz, kucharik@newton.fjfi.cvut.cz

†XCP-4 Group, MS-F644
Los Alamos National Laboratory
Los Alamos, NM 87545, USA
e-mail: shashkov@lanl.gov

Key words: Arbitrary Lagrangian-Eulerian Methods, Remap, Flux-based Remap

Abstract. In this paper, we apply the ideas of the hybrid multi-material remapping algorithm in the case of single-material discrete functions. We analyze both intersection- and swept-based remapping approaches and show that the swept-based approach can potentially produce higher numerical error and violation of solution symmetry. To fix this, we test two switches picking one or the other method, depending on the function derivatives. We demonstrate properties of both original methods and their combination on a selected numerical example.

1 INTRODUCTION

In the numerical simulations of fluid flows, the choice of the computational mesh is crucial. Traditionally, there have been two viewpoints utilizing the Lagrangian or the Eulerian framework, each with its own advantages and disadvantages. In a pioneering paper [1], Hirt et al. developed the formalism for a mesh whose motion can be determined as an independent degree of freedom, and showed that this general framework can be used to combine the best properties of the Lagrangian and Eulerian methods. This class of methods has been termed Arbitrary Lagrangian-Eulerian or ALE. Many authors have described the ALE strategies to optimize their accuracy, robustness, or computational efficiency.

It is usual to separate the ALE scheme into three distinct stages: 1) a Lagrangian stage, in which the fluid quantities and the computational mesh are advanced to the next time level; 2) a rezoning stage, in which the geometrical quality of the computational mesh

is improved; and 3) a remapping stage, in which all fluid quantities are conservatively transferred from the Lagrangian to the rezoned mesh. In this paper, we focus on the last part of the ALE scheme – the remapping stage in 2D Cartesian geometry.

For realistic simulations, multi-material ALE is typically used. In this case, more than one material is allowed in each cell of the computational mesh. Multi-material remapping typically involves intersections of the pure material polygons with the neighboring cells to construct the mass fluxes. In the series of papers [2, 3, 4], the idea of hybrid remapping is presented. The expensive intersections are used only in the vicinity of material interfaces, while a cheaper swept-based method is used in pure-material regions.

In this paper, we analyze both intersection-based and swept-based remapping methods and show that the swept-based approach can bring additional error to the remapped values in certain situations. It is therefore possible to apply the same methodology in the single-material case in order to reduce the numerical error and improve the symmetry of the remapped quantity field. We suggest two switches which alter the methods in a unified flux-based pseudo-hybrid framework and demonstrate their performance on a selected numerical example.

The rest of the paper is organized as follows. In Section 2, the standard intersection-based and swept-based remapping methods are reviewed and the idea of pseudo-hybrid remapping is introduced. In Section 3, the error analysis of both approaches is performed in a considerably simplified case and the particular terms responsible for additional numerical error of the swept-based approach are identified. In Section 4, we suggest two switches based on the first and second derivatives, choosing the appropriate methods in different parts of the domain. Both methods are compared with their pseudo-hybrid extension on a selected numerical example in Section 5. Finally, the whole paper is concluded in Section 6.

2 REMAPPING METHODS

Remapping represents a conservative transfer of all fluid quantities from the original (Lagrangian) computational mesh to the new (rezoned) one. In this paper, we only focus on the remap of a single cell-centered quantity – density ρ. For more details on the remap of the full set of fluid quantities in the same framework, see [5].

If both original and new meshes have the same topology, such as shown in Figure 1 (a), the remapping of mass in cell c can be written in a flux form

$$m_{\tilde{c}} = m_c + \sum_{c' \in C(c)} F^m_{c,c'} \,, \tag{1}$$

where $\tilde{c}$ represents the new cell, c' represents a cell from the neighborhood $C(c)$ of cell c, and $F^m_{c,c'}$ represents the mass flux from c to c'. The computation of such fluxes depends on the particular remapping method. Finally, the remapped density is obtained just by diving by the new cell volume, $\rho_{\tilde{c}} = m_{\tilde{c}}/V_{\tilde{c}}$.

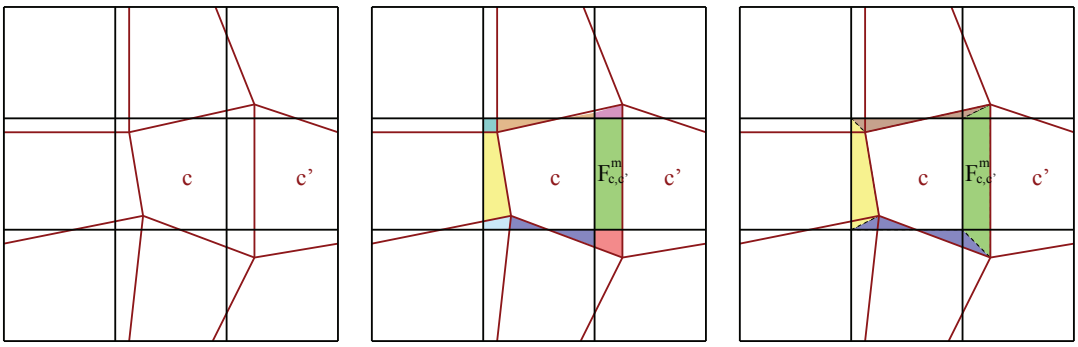

Figure 1: (a) Original (red) and rezoned (black) computational mesh. (b) Intersection-based fluxes between c and its neighbors shown in different colors. (c) Swept-based fluxes between c and its edge-neighbors shown in different colors.

2.1 Intersection-based remap

The most straightforward approach for quantity remapping is the intersection-based method, also known as overlays. For details, see for example [6, 5]. This approach can be used in the flux form (1), where the mass fluxes are computed as

$$F^m_{c,c'} = \int_{\tilde{c}\cap c'} \rho_{c'}(x,y)\,dx\,dy - \int_{c\cap\tilde{c}'} \rho_c(x,y)\,dx\,dy\,. \tag{2}$$

For an example, see Figure 1 (b). Here, the first term represents the part of the flux which needs to be added to the cell as the particular piece of the domain was added to c during the rezoning stage. Similarly, flux corresponding to the removed pieces of c is represented by the second term here. The density reconstruction $\rho_c(x,y)$ in cell c is performed by a standard piecewise-linear reconstruction process such as described in [7]. This approach is known to be conservative, consistent, linearity-preserving, second order accurate, and in the case of limited reconstruction also local-bound-preserving. On the other hand, the intersections need to be constructed, which increases the computational cost of this method significantly.

2.2 Swept-based remap

In the swept-based approach, the fluxes are approximated using swept regions instead of construction of the intersections [6, 8]. Swept region is defined by the motion of a particular cell edge during the rezoning stage, so only fluxes belonging to the edge-neighbors exist. For explanation, see Figure 1 (c). The flux form (1) can then be reduced to

$$m_{\tilde{c}} = m_c + \sum_{e\in E(c)} F^m_e\,, \tag{3}$$

where the flux through edge e is constructed as

$$F_e^m = \int_{\Omega_e} \rho_{c^*}(x,y)\,dx\,dy\,. \tag{4}$$

Here, Ω_e represents the swept region corresponding to edge e and the reconstruction is taken either from cell c or from its neighbor c' over the edge e, depending on the sign of the swept region area,

$$c^* = \begin{cases} c & \text{if} \quad V_{\Omega_e} < 0 \\ c' & \text{if} \quad V_{\Omega_e} \geq 0 \end{cases} . \tag{5}$$

This approach is significantly more efficient as no intersections are required. It is conservative, consistent, linearity-preserving, and second order accurate. On the other hand, the local-bound-preservation is not guaranteed if no additional mechanism is applied [8].

2.3 Pseudo-hybrid remap

In a series of papers [2, 3, 4], we have developed the framework of hybrid remapping for the multi-material quantity remapping. The intersection-based remap can be generalized for multiple materials in a straightforward way, while this generalization is not clear for the swept-based approach. The main idea of the hybrid remapping technique is following: perform the expensive intersections only in the vicinity of material interfaces, while cheaper swept-based remap is done in the rest of the domain.

In this paper, we incorporate the same idea for the single-material case. However, the main motivation is slightly different here. In the next Section, we analyze the errors of the intersection- and swept-remapped density values for a simplified cell motion during the rezoning stage. We demonstrate that the error of the swept-based remap contains additional terms in certain cases which can result in a higher numerical error and especially symmetry violation of the remapped values. Therefore, each of these methods can be more suitable in different parts of the computational domain. Here, we adopt the simplest two-step approach of hybrid remap [3] and combine both remapping approaches by a different criteria than the presence of the material interface – function derivatives, deviation of the function reconstruction in the neighborhood, pathological motion of the cell in the rezoning stage, etc.

The two-step hybrid remapping method does the complete Eulerian part of the ALE algorithm (rezoning+remapping) twice. First, all mesh nodes are marked as pure (all their adjacent cells are pure and contain the same material) or mixed. In the first step, only pure nodes are rezoned. This cannot affect any mixed cells so the swept-based remapping method can be used as only pure material fluxes are computed. In the second step, the remaining mixed nodes are rezoned and the intersection-based remapping method is used, which treats the multi-material fluxes properly. Let us note, that this combination keeps consistency, linearity-preservation, and the second order of accuracy of both remapping methods. Typically, it improves the computational cost of the remapper. On the other

hand, the overhead of the method involves marking of the nodes and remapping by both methods in the buffer region of cells containing both pure and mixed nodes, which can decrease the efficiency of the method in the case of more complex material interfaces.

In the pseudo-hybrid method proposed in this paper, we suggest similar combination of the intersection-based and swept-based remapping methods. However, the switch marking the nodes cannot be based on material interfaces, as we focus on single-material quantity here. Two possible switches are suggested in Section 4.

3 ERROR ANALYSIS OF REMAPPING METHODS

In papers containing the comparison of the intersection-based and swept-based remapping methods such as [6, 8, 9], the numerical errors of both approaches are comparable and the swept-based remap can be even slightly better in some cases. In [6], a basic error-analysis of both approaches is performed. The von Neumann analysis for a particular flux is performed in [10], explaining the slightly-lower numerical error of the swept-based method in the case of the traverse flows. Here, we perform similar analysis for a full quadrilateral computational cell by remapping a higher-order Taylor series using its piecewise-linear reconstruction.

Let us assume that we have a polynomial function

$$f(x,y) = C_0 + C_x\,x + C_y\,y + \frac{1}{2}\,C_{x^2}\,x^2 + C_{x\,y}\,x\,y + \frac{1}{2}\,C_{y^2}\,y^2 + \frac{1}{6}\,C_{x^3}\,x^3 + \frac{1}{2}\,C_{x^2\,y}\,x^2\,y + \frac{1}{2}\,C_{x\,y^2}\,x\,y^2 + \frac{1}{6}\,C_{y^3}\,y^3\,, \quad (6)$$

representing the third-order Taylor series centered in the origin, where the C coefficients represent the function values/derivatives. Let us construct a 5×5 equidistant uniform mesh covering the entire $\langle -\frac{5}{2}\,l_x, \frac{5}{2}\,l_x\rangle \times \langle -\frac{5}{2}\,l_y, \frac{5}{2}\,l_y\rangle$ domain, where l_x and l_y stand for the cell size in each direction. Let us perform the reconstruction in each cell by the piecewise-linear function in a least-squares manner, as described in [5]. Let us move the nodes of the central cell by same vector $[dx, dy]$, as shown in Figure 2. Now, we perform remapping of the function to the new mesh using both intersection-based and swept-based approaches. We have implemented the piecewise-linear function reconstruction and both remapping approaches in the computer algebra system Maple and are able to perform the full remap with general parameters $[l_x, l_y]$ and $[dx, dy]$. Next to it, we have confirmed the following results in a standard numerical remapping code. The 5×5 mesh is large enough to avoid any boundary effects to appear in the central cell c.

The error in cell c for the intersection-based remap can be computed as the difference between the remapped value and the analytic function evaluated in the centroid of the new cell,

$$\begin{aligned} E^{\text{int}} &= \rho_{\tilde{c}}^{\text{int}} - f(x_{\tilde{c}}, y_{\tilde{c}}) \\ &= C_{x^3}\left(\frac{l_x}{4}\,dx^2 - \frac{l_x^2}{12}\,dx - \frac{1}{6}\,dx^3\right) + C_{y^3}\left(\frac{l_y}{4}\,dy^2 - \frac{l_y^2}{12}\,dy - \frac{1}{6}\,dy^3\right). \end{aligned} \quad (7)$$

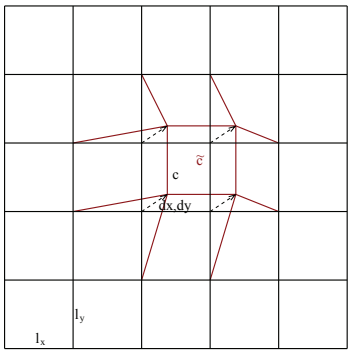

Figure 2: Original equidistant (black) and new (red) mesh. All vertices of the central cell c are shifted by $[dx, dy]$.

As we can see, the error contains only the third-order derivatives, so the intersection-based remap will be exact for a parabolic function in the special case of cell translation. Moreover, no terms containing mixed derivatives are present in the error.

Same approach can be applied for the swept-based error construction,

$$\begin{aligned} E^{\text{swept}} &= \rho_{\tilde{c}}^{\text{swept}} - f(x_{\tilde{c}}, y_{\tilde{c}}) \\ &= E^{\text{int}} + C_{x^2\,y} \left(\frac{l_x}{4}\, dx\, dy - \frac{1}{2}\, dx^2\, dy \right) + C_{x\,y^2} \left(\frac{l_y}{4}\, dx\, dy - \frac{1}{2}\, dx\, dy^2 \right) . \end{aligned} \tag{8}$$

As we can see, the error contains exactly the same terms as in the case of the intersection-based error and additional terms containing the mixed derivatives. Unfortunately, the magnitude of these error formulas depends not only on the polynomials in dx and dy (with the particular cell parameters l_x, l_y), but also on the C coefficients, which can be both positive and negative, and depend on the particular function $f(x, y)$. On the other hand, the swept-based error formula contains the same common terms as the intersections-based error formula and the extra terms which can increase its magnitude if the C coefficients have the right sign (worst case scenario). In other words, for $C_{x^3} + C_{y^3} \approx C_{x^2\,y} + C_{x\,y^2}$, both methods have comparable numerical errors. If their signs are opposite, $C_{x^3} + C_{y^3} \approx -(C_{x^2\,y} + C_{x\,y^2})$, the swept-based method always produces higher numerical error.

This conclusion is supported by the plot of the error terms shown in Figure 3 for a special case of $l_x = l_y = 1$. It is simple to investigate that (for our given mesh) the absolute value of the extra term if always slightly larger than the absolute value of the common term. Let us note, that in Figure 3, the value of $dy = 0.5$ (worst case) is assumed. For smaller values of dy, the magnitude of the extra term will decrease as it is linear in dy. On the other hand, for dy small, term opposite from (8) (with dy and dx switched) will become dominant and the extra term will become significant again. The conclusion therefore is that in the case of a computational cell translation, the terms corresponding

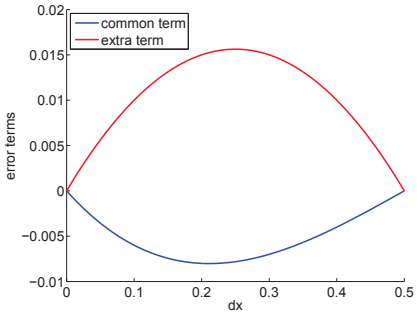

Figure 3: Plot of the common error term $\frac{dx^2}{4} - \frac{dx}{12} - \frac{dx^3}{6}$ appearing in both intersections-based and swept-based error formulas (blue line) and the additional error term $\frac{dx\,dy}{4} - \frac{dx^2\,dy}{2}$ (for a chosen value of $dy = 0.5$ representing the maximum motion) appearing only in the swept-based error formula (red line) as functions of dx.

to the mixed derivatives of the remapped function can bring significant contribution to the total error of the swept-based remapping approach, which do not show up for the intersection-based approach.

Let us remind, that this simple analysis only holds for a very special case of cell translation. For a general case of arbitrary cell deformation, we are not able to analyze the situation properly as the error formulas are too complicated. However, we are able to analyze few more simplified cases, such as cell compression/expansion, single node motion, or hourglass-type edge deformation, for which similar conclusions can be done.

4 SWITCHES OF REMAPPING METHODS

In this paper, we use two different switches for combining the intersection-based and swept-based remapping methods in different parts of the computational domain in the two-step hybrid remapping manner [3]. Let us note that these switches are constructed for educational purposes only, in reality, one can construct a switch adapted for the particular needs. We did some preliminary tests with the switches detecting standard deviation of the density error in the surrounding cells, hourglass detector, or detector of mixed derivative magnitude, for preliminary results see [11].

The first switch is inspired by the Harten-Zwas scheme [12] and utilizes the first derivative of the density function. The motivation is clear: it will trigger the intersection-based remap in regions with high gradients, detecting the function discontinuities where the swept-based remap is expected to produce maximal error. The switch is computed as

$$s_c = \frac{1}{\rho_{\max}} \sqrt{\left(\frac{\partial \rho}{\partial x}\right)_c^2 + \left(\frac{\partial \rho}{\partial y}\right)_c^2}, \tag{9}$$

where $\rho_{\max}$ stands for the maximal density in the entire domain and the density derivatives in cell c are computed by a standard piecewise-linear reconstruction technique. The switch

is compared with a threshold, typical values are between 0.1 and 10.

The second switch is based on the magnitude of the second derivative in order to detect areas of high curvature of the discrete function. It does not false trigger in regions of constant gradients. The function curvature in cell c is described by its Hessian matrix,

$$H_c = \begin{pmatrix} \left(\frac{\partial^2 \rho}{\partial x^2}\right)_c & \left(\frac{\partial^2 \rho}{\partial x \partial y}\right)_c \\ \left(\frac{\partial^2 \rho}{\partial y \partial x}\right)_c & \left(\frac{\partial^2 \rho}{\partial y^2}\right)_c \end{pmatrix}, \tag{10}$$

where the second derivatives are computed numerically from the first derivatives, using the same standard least-squares-based reconstruction technique. A local extremum is present if the matrix is positive or negative definite. To check this, we constructed a switch based on the determinant of this matrix,

$$s_c = \frac{1}{\rho_{\max}} \sqrt{\left| \left(\frac{\partial^2 \rho}{\partial x^2}\right)_c \left(\frac{\partial^2 \rho}{\partial y^2}\right)_c - \left(\frac{\partial^2 \rho}{\partial x \, \partial y}\right)_c^2 \right|}. \tag{11}$$

The higher this value is, the higher curvature is present. If a particular threshold value is reached, the intersection-based method is performed.

5 NUMERICAL EXAMPLE

In this Section, we demonstrate the performance of the remapping methods on a particular example taken from [3]. In this test, the initial cell masses are set according to a discontinuous radially-symmetric density function

$$f(x,y) = \begin{cases} 1 + e^{10\sqrt{(x-1/2)^2+(y-1/2)^2}} & \text{if } \sqrt{(x-1/2)^2+(y-1/2)^2} \le 1/4 \\ 1 + e^{6\sqrt{(x-1/2)^2+(y-1/2)^2}-1/4} & \text{otherwise} \end{cases} \tag{12}$$

in the entire $\langle 0,1\rangle^2$ domain covered by an equidistant orthogonal computational mesh containing 25^2, 50^2, 100^2, 200^2, or 400^2 cells. To enhance the effects of each remapping method, we perform the cyclic remapping test using the tensor-product mesh motion [6],

$$x_i^n = x_i^0 \left(1 - d^n\right) + \left(x_i^0\right)^3 d^n \,, \; y_i^n = y_i^0 \left(1 - d^n\right) + \left(y_i^0\right)^2 d^n \,, \tag{13}$$

$$d^n = \frac{\sin(2\pi t^n)}{2} \,, \; t^n = n/n_{\max} \,, \tag{14}$$

where (x_i^n, y_i^n) denotes the nodal position of node i in the actual remapping step n, $n_{\max}$ stands for the total number of steps, and (x_i^0, y_i^0) denotes the nodal position in the initial mesh. The number of remapping steps increases with the mesh size, $n_{\max}^{25} = 50$, $n_{\max}^{50} = 100$, $n_{\max}^{100} = 200$, $n_{\max}^{200} = 400$, $n_{\max}^{400} = 800$. This mesh motion contains a lot of cell translations (analyzed in Section 3) combined with cell compressions and expansions,

having similar effects. The same series of remapping steps is performed by all available remapping methods – intersection-based, swept-based, and the pseudo-hybrid remapping with the switches based on the first and the second derivatives from Section 4. The threshold values used in the simulations are $S^{1st\,der} = 8$ and $S^{2nd\,der} = 37$. These values were chosen heuristically to minimize the number of cells treated by the intersection-based approach while keeping good symmetry properties of the solution. In general, this test represents remapping of a symmetric function over a series of non-symmetrically moving meshes. Such situation can appear in real hydrodynamic simulations if the mesh rezoner does not take the symmetric nature of the problem into account.

Table 1: L_1 numerical error of each remapping method (intersection-based, swept-based, and pseudo-hybrid with switches based on the first/second derivatives) for different mesh resolutions.

Mesh size	Intersections	Swept	PH 1st deriv.	PH 2nd deriv.
25^2	$1.186 \cdot 10^{-1}$	$1.161 \cdot 10^{-1}$	$1.168 \cdot 10^{-1}$	$1.161 \cdot 10^{-1}$
50^2	$7.837 \cdot 10^{-2}$	$7.702 \cdot 10^{-2}$	$7.838 \cdot 10^{-2}$	$7.814 \cdot 10^{-2}$
100^2	$4.940 \cdot 10^{-2}$	$4.859 \cdot 10^{-2}$	$4.933 \cdot 10^{-2}$	$4.943 \cdot 10^{-2}$
200^2	$2.982 \cdot 10^{-2}$	$2.930 \cdot 10^{-2}$	$2.981 \cdot 10^{-2}$	$2.982 \cdot 10^{-2}$
400^2	$1.782 \cdot 10^{-2}$	$1.750 \cdot 10^{-2}$	$1.783 \cdot 10^{-2}$	$1.782 \cdot 10^{-2}$

In Table 1, we can see the total numerical error of each simulation. As the initial and final meshes coincide, the error can be computed as

$$L_1 = \frac{\sum_{\forall c} |m_c - m_c^0|}{\sum_{\forall c} m_c^0}\,, \tag{15}$$

where m_c stands for the final mass in cell c after the series of remaps and m_c^0 is the initial mass. As we can see, both intersection-based and swept-based methods exhibit comparable errors, in general, the swept-based approach is performing slightly better. This corresponds to the observations from [6, 8, 9, 10].

The density profiles are shown in Figure 4. We can see the symmetry violation of the swept-based approach, which does not show up in the intersection-based approach. This violation can be seen also for the pseudo-hybrid remaps, but it is not so significant. To confirm this observation, we calculate the relative standard deviation of the L_1 errors to express its variability over the four quadrants of the domain,

$$\sigma_{L_l} = \frac{\sqrt{\frac{1}{4}\sum_{q=1}^{4} \left(L_1^q - L_1\right)^2}}{L_1}\,, \tag{16}$$

where L_1^q represents the total mass error for a particular quadrant q and L_1 stands for the total mass error over the entire domain. The results for all remapping methods are shown

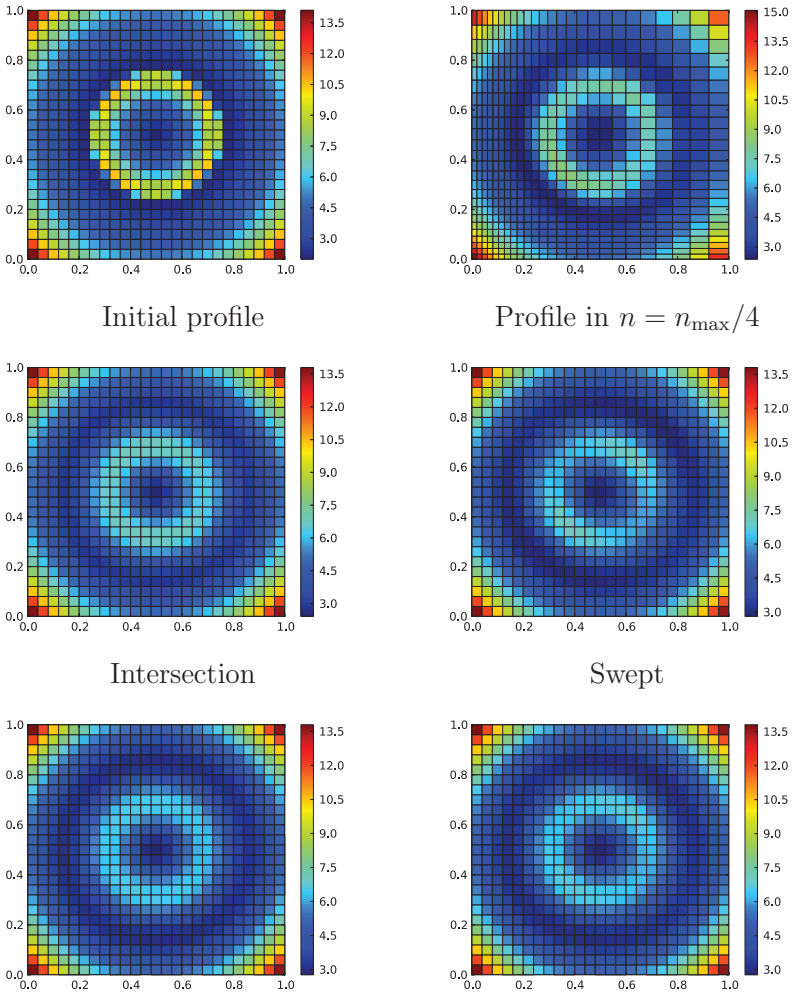

Figure 4: Initial, intermediate (maximal mesh deformation), and final density profiles for all remapping methods (intersection-based, swept-based, and pseudo-hybrid with switches based on the first/second derivatives) of double-exponential function on 25^2 mesh.

in Table 2. As we can see, the error deviation is significantly lower for the intersection-based method, so this remapping approach preserves symmetric function better than the swept based approach. This symmetry violation is caused by the terms containing mixed derivatives in equation (8). We can also see that the pseudo-hybrid methods show comparable error deviations with the intersection-based approach (for higher mesh resolutions).

Table 2: Error deviation σ_{L_1} (in %) of each remapping method (intersection-based, swept-based, and pseudo-hybrid with switches based on the first/second derivatives) for different mesh resolutions.

Mesh size	Intersections	Swept	PH 1st deriv.	PH 2nd deriv.
25^2	5.46	10.22	9.05	10.22
50^2	2.65	9.44	4.02	5.80
100^2	2.94	10.67	3.85	3.11
200^2	2.91	10.86	3.13	2.93
400^2	2.76	10.92	2.81	2.76

Let us also comment on the computational efficiency of the remapping methods. This analysis is strongly implementation-dependent and can differ significantly in different codes. In general, the intersection-based approach is the slowest one as it requires construction of the expensive cell intersections, while the swept-based approach is fastest. The pseudo-hybrid approaches contain certain overhead, as described in Section 2.3. In our code, the intersection based approach is about 4.2-times slower than the swept-based approach for the finest mesh. The pseudo-hybrid methods were about 1.8-times slower, which is significantly better than the intersection-based approach while keeping its symmetry properties.

6 CONCLUSIONS

In this paper, we analyzed the standard intersection-based and swept-based remapping techniques and identified the mixed-derivative terms responsible for the numerical error and especially symmetry violation in the case of the swept-based method. We followed the idea of hybrid remapping and suggested a combination of both approaches, which decreases these errors and improves symmetry of the remapped function. Performance of all methods was demonstrated on a static-remapping numerical test.

7 ACKNOWLEDGMENTS

This work was performed under the auspices of the National Nuclear Security Administration of the US Department of Energy at Los Alamos National Laboratory under Contract No. DE-AC52-06NA25396 and supported by the DOE Advanced Simulation and Computing (ASC) program. The authors acknowledge the partial support of the DOE Office of Science ASCR Program. This work was partially supported by the Czech Technical University grant SGS13/220/OHK4/3T/14, the Czech Science Foundation project 14-21318S and by the Czech Ministry of Education project RVO 68407700.

REFERENCES

[1] Hirt, C.W., Amsden, A.A., and Cook, J.L. An arbitrary Lagrangian-Eulerian computing method for all flow speeds. *J. Comput. Phys.* (1974) **14**:227–253.

[2] Kucharik, M., Breil, J., Galera, S., Maire, P.-H., Berndt, M., and Shashkov, M. Hybrid remap for multi-material ALE. *Comput. Fluids* (2011) **46**:293–297.

[3] Berndt, M., Breil, J., Galera, S., Kucharik, M., Maire, P.-H., and Shashkov, M. Two-step hybrid conservative remapping for multimaterial arbitrary Lagrangian-Eulerian methods. *J. Comput. Phys.* (2011) **230**:6664–6687.

[4] Kucharik, M. and Shashkov, M. One-step hybrid remapping algorithm for multi-material arbitrary Lagrangian-Eulerian methods. *J. Comput. Phys.* (2012) **231**:2851–2864.

[5] Kucharik, M. and Shashkov, M. Conservative multi-material remap for staggered multi-material arbitrary Lagrangian-Eulerian methods. *J. Comput. Phys.* (2014) **258**:268–304.

[6] Margolin, L.G. and Shashkov, M. Second-order sign-preserving conservative interpolation (remapping) on general grids. *J. Comput. Phys.* (2003) **184**:266–298.

[7] Barth, T.J. Numerical methods for gasdynamic systems on unstructured meshes. *An introduction to Recent Developments in Theory and Numerics for Conservation Laws, Proceedings of the International School on Theory and Numerics for Conservation Laws*. Springer, 1997.

[8] Kucharik, M., Shashkov, M., and Wendroff, B. An efficient linearity-and-bound-preserving remapping method. *J. Comput. Phys.* (2003) **188**:462–471.

[9] Loubere, R. Private communication, (2013).

[10] Lauritzen, P.H., Erath, Ch., and Mittal, R. On simplifying 'incremental remap'-based transport schemes. *J. Comput. Phys.* (2011) **230**:7957–7963.

[11] Klima, M. *Pseudo-hybrid remapping*. Technical report, Czech Technical University in Prague, (2013).

[12] Laney, C.B. *Computational Gasdynamics*. Cambridge University Press, (1998).